Salt-Induced Oligomerization of Partially Folded Intermediates of Equinatoxin II[†]

Nataša Poklar Ulrih,*[,‡] Gregor Anderluh,[‡] Peter Maček,[‡] and Tigran V. Chalikian*[,§]

Biotechnical Faculty, University of Ljubljana, Jamnikarjeva 101, 1000 Ljubljana, Slovenia, and Department of Pharmaceutical Sciences, Leslie Dan Faculty of Pharmacy, University of Toronto, 19 Russell Street, Toronto, Ontario, Canada M5S 2S2

Received February 24, 2004; Revised Manuscript Received May 21, 2004

ABSTRACT: Equinatoxin II (EqTxII) is a cytolytic, water-soluble protein which binds to and forms cation-selective pores in lipid membranes. To characterize the native and denatured states of EqTxII and to elucidate the biological role of its oligomers, we have studied salt-dependent heat-induced conformational transitions of EqTxII. To this end, we have employed a variety of experimental techniques, including differential scanning calorimetry, circular dichroism and light absorption spectroscopy, ultrasonic velocimetry, electron microscopy, PAGE, and a hemolytic activity assay. This experimental combination has enabled us to monitor and structurally and thermodynamically characterize temperature-induced conformational transitions and oligomerization of EqTxII at different concentrations of NaCl. At pH 3.0 and 25 °C, EqTxII retains its native conformation and remains hemolytically active over a broad range of NaCl concentrations. However, an increase in the salt concentration results in a diminution of the thermal stability of EqTxII. Specifically, the calorimetrically determined denaturation temperature, T_d, and enthalpy, ΔH_{cal}, of the toxin decrease with an increase in the salt concentration. Our CD data suggest that the heat-induced denatured state of EqTxII lacks rigid tertiary structure while exhibiting well-defined secondary structure. The amount of the induced, non-native secondary structure of EqTxII depends on the solution ionic strength, temperature, time of incubation at an elevated temperature, and protein concentration. Our combined results suggest that, in the presence of salt, an increase in temperature results in formation of the partially unfolded state of the toxin that oligomerizes and forms biologically inactive, water-soluble aggregates.

Pore-forming peptides and proteins have been discovered in a wide range of organisms, including bacteria, plants, fungi, primitive metazoans, insects, and mammals. These toxins exist as either monomers or water-soluble oligomers and exert their toxic effects by interacting with and forming pores in lipid membranes of the target organism (*1*, *2*). Sea anemones produce one or more ∼20 kDa cytolysins that belong to a protein family broadly termed actinoporins (*3*). Actinoporins are known to permeabilize model lipids and cell membranes (*4*, *5*). All actinoporins studied to date [such as equinatoxin II (EqTxII)[1] and sticholysin I and II] are able to adopt partially unfolded conformational states under appropriate solution conditions. These states are structurally and thermodynamically distinct from the fully unfolded state and exhibit markedly reduced biological activity (*6*−*12*). At extremes of pH, EqTxII adopts a partially unfolded conformation with well-defined secondary structure and no rigid tertiary structure (*10*). In this state, the toxin oligomerizes and forms water-soluble aggregates (*10*).

[†] This work was supported by a NATO Collaborative Linkage Grant (LST.CLG 974812).

* To whom correspondence should be addressed. N.P.U.: fax, +386 1 256 6296; telephone, +386 1 423 1161; e-mail, natasa.poklar@uni-lj.si. T.V.C.: fax, +416 978 8511; telephone, +416 946 3715; e-mail, chalikan@phm.utoronto.ca.

[‡] University of Ljubljana.

[§] University of Toronto.

[1] Abbreviations: ANS, 1-anilinonaphthalene-8-sulfonic acid ammonium salt; BRBC, bovine red blood cells; CD, circular dichroism; DSC, differential scanning calorimetry; EqTxII, equinatoxin II; PAGE, polyacrylamide gel electrophoresis; T_d, denaturation temperature.

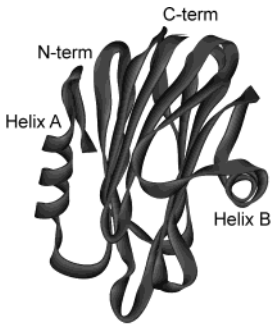

FIGURE 1: Ribbon diagram of the EqTxII structure (*32*).

Although exact mechanisms of pore formation by actinoporins are poorly understood, it is believed that trimerization or tetramerization of EqTxII precedes its binding to the cell membrane and subsequent formation of cation-selective pores with an estimated functional diameter of ∼2 nm (*5*). Insertion of an EqTxII molecule into a lipid membrane is modulated by the lipid composition, surface charge, and physical state of the latter (*5*, *13*, *14*). Interestingly, at low protein-to-lipid molar ratios ($R < 0.05$), anionic membranes in their liquid-crystalline state trigger a β-to-α transformation of EqTxII (Figure 1). At higher R values, the protein−lipid complex precipitates (*13*). Binding of EqTxII to lipid membranes proceeds in two steps [the binding-induced partial unfolding of EqTxII is followed by its oligomerization and insertion into the membrane (*2*)] which are mediated by two structural regions of the toxin (*15*). The first region consists of solvent-exposed, tryptophan-contain-

10.1021/bi049616h CCC: $27.50
Published on Web 06/29/2004

ing aromatic clusters, while the second region is represented by the N-terminal amphiphilic helix which subsequently tranclocates into the lipid phase (*16*). It should be noted, however, that some bacterial pore-forming toxins may bind as a monomer and then undergo partial unfolding triggered by a local acidic pH near negatively charged membrane surfaces (*17*−*21*).

To further investigate the oligomerization of partially unfolded (presumably, molten globule-like) states of EqTxII, we have studied in this work the effect of NaCl on the thermodynamic and conformational properties of EqTxII at pH 3.0. To this end, we have employed a combination of calorimetric (DSC), spectroscopic (CD and UV), volumetric (ultrasonic velocimetry), microscopic (electron microscopy), and electrophoretic (native PAGE) techniques. Our data suggest that, at pH 3.0 and high salt concentrations, the heat-induced partially unfolded state of EqTxII oligomerizes and forms non-native α-helical secondary structure. We propose that this non-native oligomeric structure of the toxin correlates with its pore forming ability.

EXPERIMENTAL PROCEDURES

Materials

EqTxII was isolated from the sea anemone *Actinia equina* L. as previously described (*22*) and stored freeze-dried at −10 °C. CsCl, NaCl, and diglycine were purchased from Sigma-Aldrich Canada (Oakville, ON). The protein was dissolved in a 10 mM diglycine buffer adjusted to pH 3.0 and dialyzed overnight against the same buffer. The concentrated solution of NaCl or CsCl in a 10 mM diglycine buffer (pH 3.0) was added to the EqTxII solution adjusted to the desired ionic strength. The concentration of EqTxII was determined spectrophotometrically using an extinction coefficient, ϵ_{280}, of 1.87 cm^{-1} L g^{-1} at 25 °C (*7*). For all the ultrasonic, CD spectroscopic, gel electrophoresis, and DSC measurements reported here, the EqTxII concentration was between 0.5 and 0.7 mg/mL (25−35 μM), while the UV melting experiments were performed at ∼0.1 mg/mL (5 μM).

Methods

CD Spectroscopy. CD spectra of EqTxII were recorded using an AVIV model 62A DS spectropolarimeter (Aviv Associates, Lakewood, NJ). Optical cuvettes with path lengths of 1 and 10 mm were employed for the far-UV (200−250 nm) and near-UV (250−310 nm) CD measurements, respectively. The CD spectra were recorded either as a function of temperature between 5 and 95 °C with a step of 5 °C or as a function of ionic strength by incrementally adding aliquots of NaCl to a cuvette containing a known amount of EqTxII at 25, 40, and 50 °C. The mean residue ellipticity, $[\theta]_\lambda$, was calculated as described previously (*7*). Deconvolution of the CD spectra was carried out using Contin's simulation (*23*).

UV Spectroscopy. UV light absorption measurements were conducted using an Aviv model 14DS UV−vis spectrophotometer equipped with a thermoelectrically controlled cell holder (Aviv Associates). The absorption versus temperature profiles of EqTxII were measured at 232 or 293 nm. The temperature was increased in a 1 °C increment, and the protein samples were allowed to equilibrate for 1 min at each temperature setting. We used the temperature-induced denaturation profiles of EqTxII to determine transition temperatures, T_d, as a function of ionic strength.

Differential Scanning Calorimetry (DSC). Calorimetric thermograms were determined using a CSC model 6100 Nano DSC differential scanning calorimeter (Calorimetry Science Corp., Provo, UT). Protein samples (∼0.5 mg/mL) in a 10 mM diglycine buffer (pH 3.0) at different concentrations of NaCl (from 0 to 200 mM) were loaded into the calorimetric cell, and each sample was heated and cooled repeatedly within the temperature range of 0−95 °C. The heating or cooling rate was 1 °C/min. The first DSC scan was used to obtain the denaturation temperature (T_d), the model-independent calorimetric enthalpy (ΔH_{cal}), and the model-dependent van't Hoff enthalpy (ΔH_{vH}), as previously described (*24*). Subsequent scans were used to assess the reversibility of protein denaturation.

Ultrasonic Velocimetry. The sound velocity in protein solutions was measured at 7.5 MHz with an ultrasonic resonator cell equipped with lithium niobate piezotransducers and with a minimum sample volume of 0.8 cm^3 (*25*−*27*). For this type of acoustic resonator, the relative precision of sound velocity measurements at frequencies near 7.5 MHz is at least $\pm 1 \times 10^{-4}$% (*28*, *29*). The key characteristic of a solute directly derived from ultrasonic measurements is the relative specific sound velocity increment ([u]), which is equal to $(U - U_0)/(U_0 c)$, where c is the specific concentration of a solute and U and U_0 are the sound velocities in the solution and solvent, respectively. Temperature-dependent ultrasonic measurements were performed in a 10 mM diglycine buffer (pH 3.0) containing 0 or 200 mM CsCl between 20 and 65 °C with an increment of 5 °C. Salt titration experiments were carried out at 25 and 50 °C by adding equal amounts of a CsCl solution to both the sample and reference cell, each containing 1.0 cm^3 of the protein solution and neat buffer, respectively. When calculating the relative specific sound velocity increment ([u]), we took into account the changes in sound velocity in the solvent and protein concentration which resulted from addition of the titrant.

Hemolytic Activity Assay. The hemolytic activity of EqTxII was measured turbidimetrically in bovine red blood cells (BRBC) at 25 °C using an MRX microplate reader (Dynex Technologies, Denkendorf, Germany). After being incubated under different conditions (NaCl concentration, temperature, and time), the toxin was added to the well with the erythrocyte buffer [0.13 M NaCl and 0.02 M Tris-HCl (pH 7.4)] and then serially diluted 2-fold. One hundred microliters of BRBC ($A_{630} = 0.5$) in the erythrocyte buffer was added to the toxin solution in each well, and hemolysis was followed turbidimetrically at 630 nm for 20 min at room temperature. The final volume in all wells was 200 μL. The maximum rate of hemolysis (ΔA_{630} per minute) was calculated for each dilution. In addition, from dose−response curves, we determined c_{50}, the toxin concentration at which the hemolysis rate equals 50% of the maximum value.

Native Gel Electrophoresis. Native PAGE was performed on a PHAST system (Amersham Pharmacia Biotech, Uppsala, Sweden) using 20% gels and reverse electrodes according to instructions provided by the manufacturer. The EqTxII samples in a 10 mM diglycine buffer (pH 3.0) and 0 and 100 mM NaCl were preincubated for different periods

of time at 50 °C in a water bath. Periodically, aliquots of EqTxII were removed from the bath, cooled to 25 °C, diluted with the same volume of sample buffer [0.224 M Tris-HCl and 0.224 M sodium acetate (pH 6.4), with crystal violet as a tracking dye], and kept at 4 °C. Shortly after removal of the last aliquot of EqTxII that had been preincubated at 50 °C, all toxin samples were applied to the gel. After electrophoresis, gels were stained with Coomassie blue and protein bands were quantified using an UVItec documentation system (UVItec Ltd., Cambridge, England).

Electron Microscopy. Electron microscopy was used to analyze EqTxII oligomers formed in the presence of 100 mM NaCl at pH 3.0 and 65 °C and at pH 1.2 and 25 °C. Transmission electron microscopy was performed with a Philips model CM100 microscope operating at 80 kV (Philips Electronics). A drop of the sample was deposited on the copper grids coated with Formvar film and negatively stained with 1% phosphotungstic acid. Samples were dried on air before imaging. Images were taken with a BioScan (Washington, DC) model 792 camera with CCD resolution at 1024 pixels × 1024 pixels.

RESULTS AND DISCUSSION

NaCl Destabilizes the Tertiary Structure and Stabilizes the Non-Native Secondary Structure of EqTxII. The near- and far-UV CD spectra of EqTxII at pH 3.0 and different NaCl concentrations were recorded between 5 and 95 °C. At pH 3.0 and 25 °C, EqTxII is in its native state and does not precipitate with an increase in temperature (*10*). Above pH 6, however, EqTxII precipitates at elevated temperatures (*7*).

Heat-induced conformational transitions of EqTxII can be monitored by plotting its molar ellipticity at selected wavelengths against temperature as shown in panels A and B of Figure 2. Inspection of Figure 2A reveals that, at all ionic strengths studied in this work, EqTxII undergoes a cooperative heat-induced transition that is accompanied by disruption of its native tertiary structure. Judging by a decrease in T_d, an increase in the NaCl concentration from 0 to 50 mM results in slight destabilization of the tertiary structure of EqTxII. A further increase in the salt concentration does not strongly influence the stability of the toxin (see Table 1).

Inspection of Figure 2B reveals that the secondary structure of EqTxII is also affected by temperature. Specifically, a monotonic increase in the ellipticity at 217 nm with temperature suggests a noncooperative disruption of the secondary structure of the toxin. Interestingly, the transition midpoint increases with an increase in NaCl concentration, suggesting that salt stabilizes the secondary structure of EqTxII (Figure 2B). In fact, in the presence of salt, the transition remains incomplete even at 95 °C, the highest temperature investigated in this work. Comparison of panels A and B of Figure 2 reveals that, in the absence of salt, the transition profiles of EqTxII monitored at 275 and 217 nm yield similar denaturation temperatures (~50 °C), although the transition monitored at 217 nm is much broader. By contrast, in the presence of NaCl, the transition profiles monitored at 275 and 217 nm are significantly different with respect to their temperature regimes.

Figure 2C depicts the far-UV CD spectra of EqTxII at 65 °C at different NaCl concentrations. At this temperature,

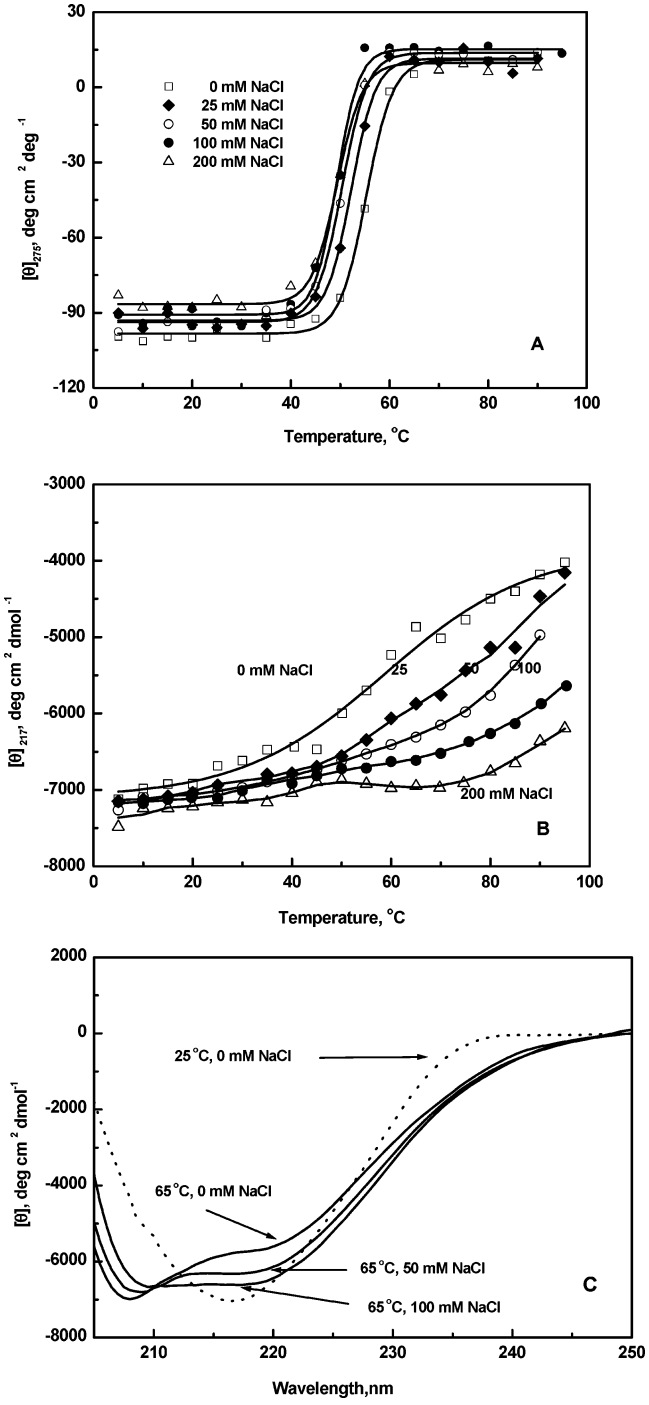

FIGURE 2: Thermally induced denaturation profiles of EqTxII at pH 3.0 and various NaCl concentrations monitored by CD ellipticity at 275 (A) and 217 nm (B). (C) Far-UV CD spectra of the native (25 °C, no salt) and heat-induced denatured (65 °C, various NaCl concentrations) states of EqTxII. All spectra were recorded at pH 3.0 in 10 mM diglycine buffer.

EqTxII lacks rigid tertiary structure (see Figure 2A) while exhibiting enhanced, non-native α-helical structure as can be judged by the two characteristic minima at 208 and 220 nm (see Figure 2C). The fraction of α-helical structure increases from ~12 to ~ 30% with an increase in ionic strength from 0 to 200 mM. Above 300 mM NaCl, EqTxII precipitates.

Our analysis of the secondary structural preferences of the polypeptide chain (as described in refs *30* and *31*) identifies several domains of the toxin molecule that may potentially

Table 1: Denaturation Temperatures, T_d, of the Thermally Induced Transitions of EqTxII As Obtained by Employing Different Techniques and the Thermodynamic Characteristics of the Thermally Induced Transitions of EqTxII at pH 3.0 (10 mM diglycine buffer) in the Presence of Different Concentrations of NaCl Obtained from DSC Measurements[a]

C_{NaCl} (mM)	$T_d(UV_{232})$ (°C)	$T_d(CD_{275})$ (°C)	$T_d(CD_{208})$ (°C)	T_d(DSC) (°C)	ΔH_{cal} (kcal/mol)	ΔH_{vH} (kcal/mol)	ΔC_p (kcal mol^{-1} K^{-1})
0	50.7 ± 0.5	55.3 ± 0.5	56.0 ± 0.5	56.9 ± 0.5	87 ± 5	93 ± 5	2.8 ± 0.5
25	48.0 ± 0.5	52.3 ± 0.5	54.5 ± 0.5	54.4 ± 0.5	60 ± 5	76 ± 5	2.3 ± 0.5
50	46.5 ± 0.5	50.4 ± 0.5	52.1 ± 0.5	53.6 ± 0.5	57 ± 5	75 ± 5	2.0 ± 0.5
100	45.2 ± 0.5	49.3 ± 0.5	52.2 ± 0.5	53.3 ± 0.5	54 ± 5	73 ± 5	1.5 ± 0.5
200	44.5 ± 0.5	49.4 ± 0.5	50.8 ± 0.5	53.3 ± 0.5	48 ± 5	65 ± 5	1.2 ± 0.5

[a] $T_d(UV_{232})$ is the denaturation temperature obtained from UV melting experiments at 232 nm. $T_d(CD_{275})$ and $T_d(CD_{208})$ are the denaturation temperatures obtained from CD melting profiles followed at 275 and 208 nm, respectively. T_d(DSC) is the denaturation temperature. ΔH_{cal} is the model-independent calorimetric enthalpy of denaturation at T_d. ΔH_{vH} is the model-dependent van't Hoff enthalpy of denaturation. ΔC_p is the difference in molar heat capacity between the denatured and native states of EqTxII. All values were obtained from DSC thermograms.

adopt an alternative, α-helical structure, thereby enhancing the α-helical content of the partially unfolded state of EqTxII (*12*, *32*). Specifically, the intrinsic propensities of the N-terminal domain, including amino acid residues 1−17, as well as residues 45−53 and 83−94, are distinct from those observed in the X-ray and/or NMR structures of the toxin (*12*, *32*). The preferred conformation of these residues is an α-helix. However, in the protein, residues 1−17 form aperiodic structure except for the short *β*-strand formed by residues 7−10, while residues 45−53 and 83−94 are in a *β*-structure (*12*, *32*).

Formation of non-native α-helical structure may, in part, result from the salt-induced aggregation of the protein at elevated temperatures as was observed for the acid-induced denatured state of EqTxII at pH 1.0 (*10*). EqTxII exhibits an isoelectric point of 10.5. Consequently, at neutral pH, EqTxII carries a positive charge. With an increase in salt concentration, electrostatic repulsion between colliding protein molecules is weakened due to charge screening, and EqTxII becomes prone to aggregation.

Analysis of the far-UV CD spectra presented in Figure 2C suggests that, at high salt concentrations and elevated temperatures, EqTxII exhibits a pronounced increase in the level of α-helical structure, a slight increase in the level of *β*-structure, and a decrease in the level of unordered structure. These observations may suggest that the rigid hydrophobic core of the protein either collapses (becomes molten globule-like) or becomes involved in formation of intermolecular contacts between aggregating protein molecules. Under similar experimental conditions, we have previously shown that heat-induced denatured state of EqTxII binds ANS, a hydrophobic probe, with high affinity (*7*). However, ANS binds equally well to nonpolar regions of monomeric and oligomeric proteins (*33*). Therefore, ANS binding results do not enable one to reliably answer the question of whether the denatured state of EqTxII is monomeric or oligomeric. In addition, it has been reported that ANS may induce protein folding (*34*, *35*) and stimulate hemolytical activity of EqTxII (*36*), experimental observations that further complicate interpretation of ANS binding experiments.

Finally, it should be pointed out that, as for EqTxII, melittin, a pore-forming peptide from bee venom, is prone to oligomerization. This observation is significant since, in addition to functional similarity, melittin exhibits amino acid sequence homology with the N-terminal domain of EqTxII (*37*). When the net charge of melittin is reduced due to salt or pH, it forms an α-helix-rich tetrameric structure (*38*).

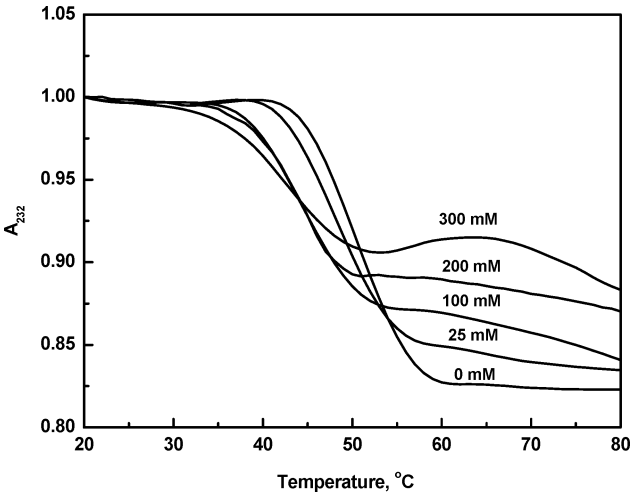

FIGURE 3: UV light absorbance of EqTxII at 232 nm, A_{232}, as a function of temperature at pH 3.0 (10 mM diglycine buffer) and different concentrations of NaCl as marked.

Heat-Induced Denaturation of EqTxII in the Presence of NaCl As Detected by UV Melting, Sound Velocity, and DSC Experiments. Figure 3 presents the UV melting profiles of EqTxII at 232 nm in a pH 3.0 buffer containing 0, 25, 100, 200, and 300 mM NaCl. Inspection of Figure 3 reveals that, in the presence of NaCl, EqTxII melts in two steps. An increase in NaCl concentration brings about a decrease in the denaturation temperature, T_d, and an increase in hyperchromicity of the first transition (see Table 1). The second transition begins prior to the completion of the first one. Above 300 mM NaCl, EqTxII precipitates before the first heat-induced transition is complete.

Figure 4 depicts changes in the relative specific sound velocity increment ([u]) of EqTxII at 0 (□) and 100 mM CsCl (■) plotted against temperature. Inspection of Figure 4 reveals that the relative specific sound velocity increment ([u]) of EqTxII depends on temperature and salt. In the absence of salt, the value of [u] cooperatively decreases between 45 and 55 °C, a range corresponding to the heat-induced denaturation of EqTxII. The pre- and post-transitional baselines of [u] are virtually independent of temperature. At 100 mM CsCl, the heat-induced denaturation of the toxin also causes a cooperative (sigmoidal) decrease in [u] at around 50 °C. However, the pre- and post-transitional baselines steeply decrease with an increase in temperature. One may plausibly propose that the post-transitional decrease in [u] reflects oligomerization of the toxin.

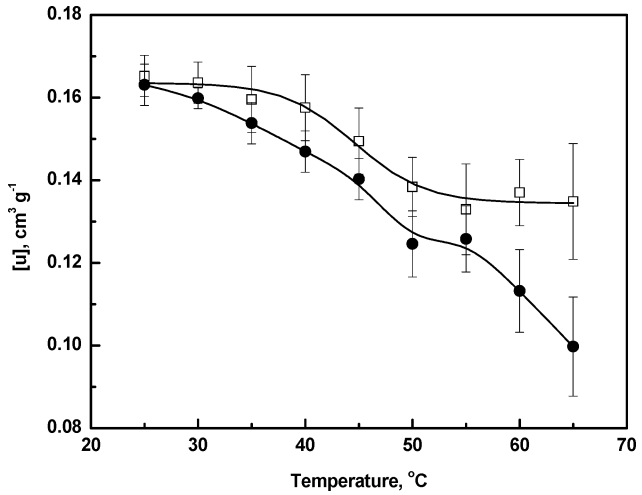

FIGURE 4: Relative specific sound velocity increment ([u]) of EqTxII as a function of temperature in the absence of salt (□) and with 100 mM CsCl (●).

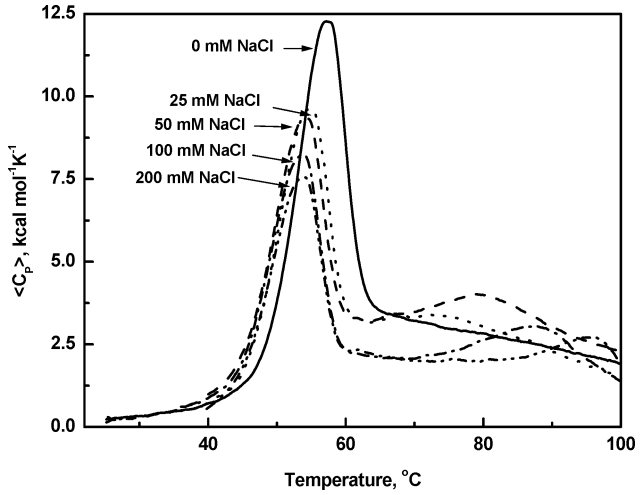

FIGURE 5: DSC melting profiles of EqTxII at different NaCl concentrations (as marked).

Figure 5 presents the DSC thermograms of EqTxII measured at different ionic strengths (between 0 and 200 mM NaCl). In the absence of salt, EqTxII manifests a single transition, an observation consistent with our CD and UV absorption data. In the presence of salt, the DSC curves presented in Figure 5 reveal two endothermic transitions. This observation is also consistent with our spectroscopic data. The calorimetrically determined denaturation temperatures (T_d) and enthalpies (ΔH_{cal}) are listed in Table 1. Inspection of data in Table 1 reveals that T_d, ΔH_{cal}, and ΔC_p of the first transition decrease with an increase in NaCl concentration.

The calorimetric enthalpy (ΔH_{cal}) of the single transition in the absence of salt is equal to 87 kcal/mol. This value coincides (within experimental error) with 93 kcal/mol, the van't Hoff enthalpy calculated from the shape of the calorimetric melting curve. This agreement suggests that, in the absence of salt, the heat-induced denaturation of EqTxII is a two-state process. In the presence of salt, however, the thermally induced denaturation of EqTxII ceases to be two-state. In all cases, the van't Hoff enthalpy (ΔH_{vH}) of the first heat-induced transition of EqTxII in the presence of salt is higher than the calorimetric enthalpy (ΔH_{cal}). Specifically, at 25, 50, 100, and 200 mM NaCl, the ratio $\Delta H_{vH}/\Delta H_{cal}$ equals 1.27, 1.32, 1.35, and 1.35, respectively. The discrepancy between ΔH_{cal} and ΔH_{vH} is consistent with the initial denaturation of the toxin followed by aggregation. The propensity of the heat-induced denatured state of EqTxII to aggregate increases with an increase in NaCl concentration as revealed by our PAGE data (not shown). This observation correlates with an increase in the $\Delta H_{vH}/\Delta H_{cal}$ ratio, a decrease in ΔC_p, and formation of non-native α-helical secondary structure as revealed by our far-UV CD spectroscopic data (see Figure 2C). It should be noted that this behavior of EqTxII is not unusual since self-association of denatured proteins often facilitates formation of non-native (mostly, α-helical) secondary structures (*39*, *40*).

The second heat-induced transition of EqTxII (see Figures 2B, 3, and 5) probably reflects further disruption of partially unfolded EqTxII oligomers containing significant amounts of non-native secondary structure. Alternatively, this transition may be related to formation of even larger oligomers.

Oligomerization of EqTxII Is Irreversible. The ratio of the calorimetric enthalpies of the second to the first heating cycles provides one means for evaluating the reversibility of a transition. Judging by this criterion, the heat-induced formation of water-soluble aggregates of EqTxII in the presence of NaCl is irreversible (data not shown). In the absence of salt, the degree of reversibility of EqTxII denaturation is a function of the uppermost temperature to which the sample has been heated. If an EqTxII sample is heated to only ~10 °C above T_d, the transition is ~90% reversible. However, if the heating proceeds to 95 °C, the transition becomes virtually irreversible (data not shown).

In the presence of NaCl, the first heat-induced transition of EqTxII is irreversible even if the heating is interrupted immediately after the transition. In contrast, the second transition that occurs at a higher temperature is invariably reversible. We propose that the oligomers, which are formed during or immediately after the first transition, undergo a reversible endothermic transition at higher temperatures. The second transition may correspond to the partial unfolding or dissociation of the oligomeric structures. This notion is consistent with our far-UV CD data which have revealed a decrease in the level of secondary structure (Figure 2B). It should be noted that the base-induced denaturation of EqTxII at room temperature is also accompanied by two transitions, of which only the second is reversible (*10*). Consequently, the base-, acid-, and heat-induced (in the presence of NaCl) conformational transitions of EqTxII are virtually irreversible.

The Oligomeric State of EqTxII Is Made of Partially Unfolded Intermediates. To identify and characterize the conformational states of EqTxII which ultimately cause its oligomerization, we have performed CD spectroscopic, ultrasonic velocimetric, PAGE, and hemolytic assay measurements in the presence and absence of NaCl. These measurements have been carried out at 25 °C (native state), 40 °C (before the transition), and 50 °C (the transition region). The far- and near-UV CD spectra of EqTxII have been measured between 0 and 500 mM NaCl. At pH 3.0 and 25 °C, the far- and near-UV CD spectra of EqTxII do not change appreciably with an increase in salt concentration from 0 to 500 mM (see Figure 6A,B). This observation suggests that, at room temperature, secondary and tertiary

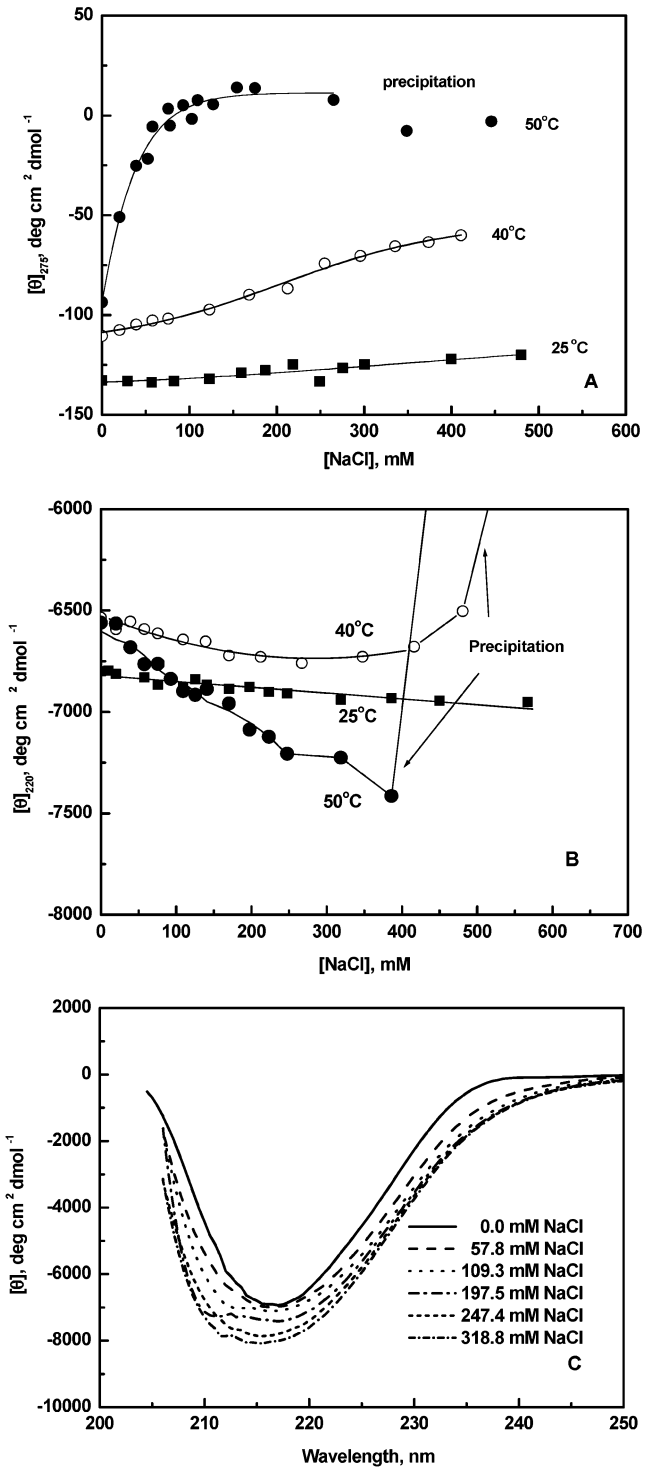

FIGURE 6: (A) Salt dependences of the molar ellipticity of EqTxII at 275 nm and 25 (■), 40 (○), and 55 °C (●). (B) Salt dependences of the molar ellipticity of EqTxII ot 220 nm and 25 (■), 40 (○), and 55 °C (●). (C) Far-UV CD spectra of EqTxII at 50 °C, pH 3.0, and different NaCl concentrations.

structures of EqTxII are not strongly affected by NaCl (Figure 6A,B).

At 25 °C, the relative specific sound velocity increment ([u]) of EqTxII linearly increases with an increase in NaCl concentration (Figure 7). An increase in [u] is consistent with protein dehydration that accompanies a salt-induced reduction in water activity (*41*).

The hemolytic activity assay of EqTxII preincubated at different concentrations of NaCl for 60 min at 25 °C does

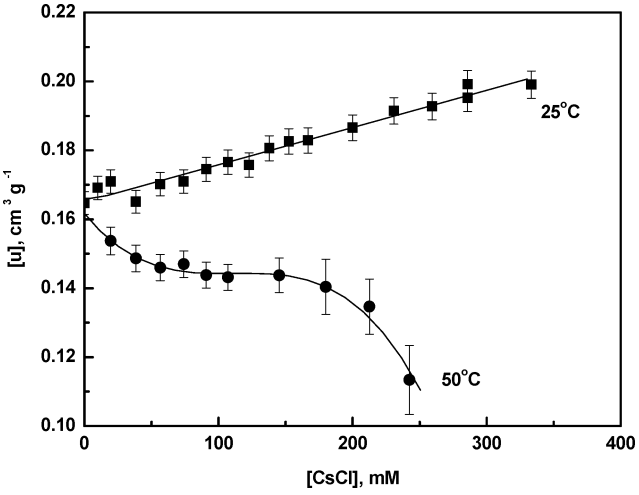

FIGURE 7: CsCl dependences of the relative specific sound velocity increment ([u]) of EqTxII at 25 (■) and 50 °C (●).

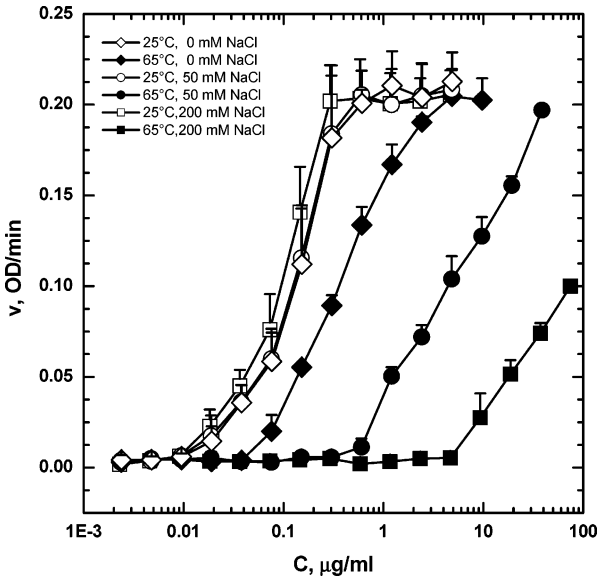

FIGURE 8: Rate of hemolysis of bovine red blood cells by EqTxII at pH 3.0 in the presence of different concentrations of NaCl as a function of toxin concentration. EqTxII was preincubated at 25 °C in the absence of salt (◇), with 50 mM NaCl (○), or with 200 mM NaCl (□) and at 65 °C in the absence of salt (◆), with 50 mM NaCl (●), or with 200 mM NaCl (■).

not reveal any significant influence of NaCl on toxin activity (see Figure 8). In contrast, toxin samples preincubated at 65 °C exhibit a strong salt dependence of their hemolytic activity. Inspection of Figure 8 reveals that the protein samples preincubated at 65 °C in the absence of salt retain 35% of their original hemolytic activity, whereas incubation at 65 °C and 50 and 200 mM NaCl reduces the hemolytic activity by 2 and 3 orders of magnitude, respectively. These observations correlate with the oligomeric state of the protein. Specifically, our PAGE results suggest that, at 25 °C, EqTxII retains its monomeric state at any NaCl concentration, while, at elevated temperatures, the toxin forms oligomers in the presence of salt (data not shown).

Inspection of Figure 6A reveals that, at 50 °C (●), the protein ellipticity at 275 nm is salt-dependent. The steep increase and leveling off of $[\theta]_{275}$ reflect the salt-induced decrease in the denaturation temperature, T_d, of EqTxII (see

Table 1). On the basis of our near-UV CD measurements, T_d decreases from 55.3 °C in the absence of salt to 49.4 °C at 200 mM NaCl (see Figure 2a). Thus, the initial increase in $[\theta]_{275}$ at 50 °C in Figure 6A reflects the salt-induced denaturation of the protein. Importantly, the salt-induced denaturation of EqTxII at 50 °C is accompanied by some enhancement in secondary structure as revealed by a shift of the far-UV CD spectrum of EqTxII to more negative values (see Figure 6B,C). In addition, we found that the amount of non-native secondary structure of the heat-induced denatured oligomeric state of EqTxII increases with salt concentration.

Further inspection of panels A and B of Figure 6 reveals that, at 40 °C, the molar ellipticities of the toxin at 220 and 275 nm exhibit some salt dependence. However, even at the highest salt concentration employed in this study, the protein remains intact at 40 °C. Precipitation of EqTxII as detected by a sharp increase in $[\theta]_{220}$ above 500 mM NaCl is likely to result predominantly from "salting out" rather than from oligomerization of the protein which is observed at 50 °C (see Figire 6B).

Inspection of Figure 7 reveals that the salt-induced denaturation of EqTxII at 50 °C (●) is accompanied by an initial exponential-like decrease in the relative specific sound velocity increment, [u] (between 0 and 100 mM CsCl), followed by a steeper decrease at higher salt concentrations. The latter result reflects precipitation of denatured EqTxII. In fact, the salt-induced formation of fibrilar oligomeric EqTxII structures at 65 °C can also be observed under the electron microscope (see Figure 9A). Significantly, the fibrils appear to be identical to those observed for the acid-induced denatured state of EqTxII at 25 °C and pH 1.2 (see Figure 9B).

To investigate how oligomerization of the toxin is modulated by its concentration, we have performed, at 50 °C, salt titration of the toxin at different concentrations and followed the ensuing oligomerization by the far-UV CD measurements (data not shown). These measurements have revealed that the concentration of NaCl needed to induce EqTxII oligomerization decreases with an increase in protein concentration.

Denatured proteins generally tend to aggregate (*20*, *42*−*49*). From this point of view, formation of oligomers by denatured EqTxII is not unexpected. In addition, it has been recently proposed that protein aggregation may facilitate formation of non-native secondary structural elements (*40*, *48*). A survey of the literature reveals that pore-forming proteins are particularly prone to oligomerization under various experimental conditions (*50*, *51*). This tendency may, in part, correlate with the mechanisms of toxicity of pore-forming proteins. For instance, pneumolysin is able to form oligomeric structures, a feature mediated by domain IV (*50*). The crystal structure of EqTxII reveals a high degree of similarity with β-sandwich domain IV of pneumolysin which is essential for its interaction with membranes (*32*). In pneumolysin, the structural change accompanying protein association is subtle, while the change in protein activity is quite dramatic (*52*, *53*). The ability of β-sandwich structures to form continuous intermolecular aggregates and insoluble amyloid fibrils has also been reported for the heptamerizing protective agent of *Bacillus anthracis* (*54*) and the α-toxin of *Staphylococcus aureus* (*55*).

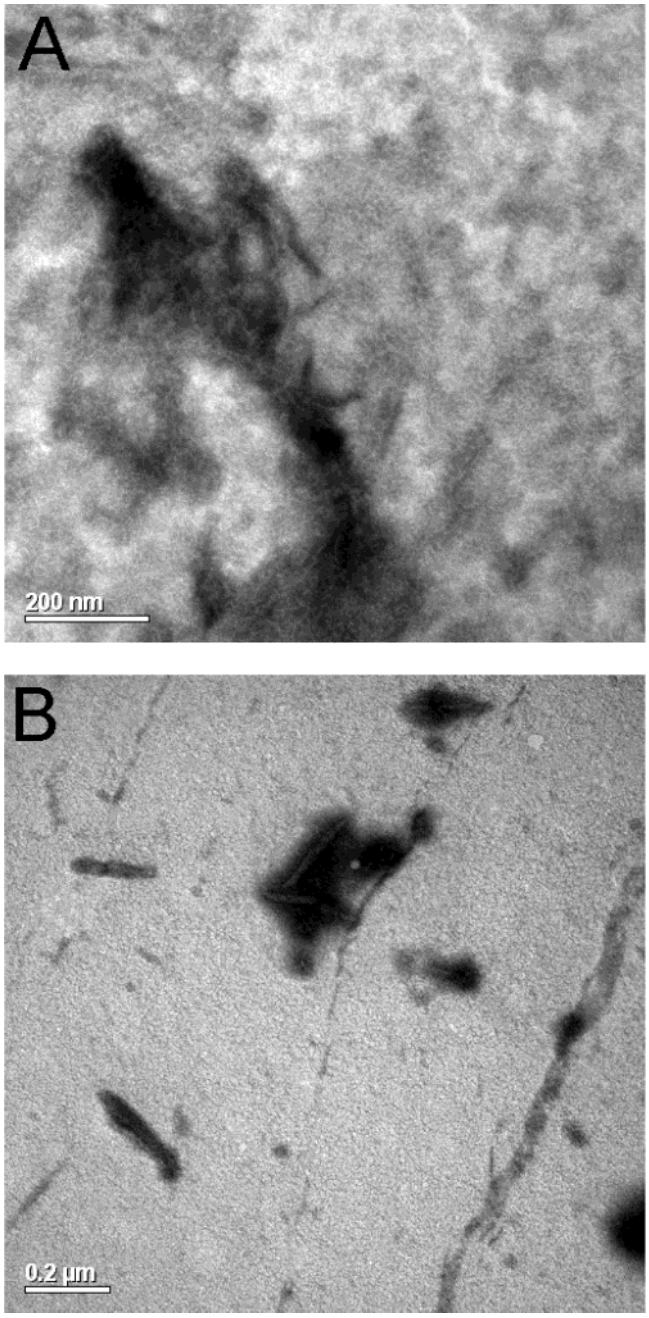

FIGURE 9: (A) Electron micrograph of thermally denatured EqTxII at 65 °C in the presence of 100 mM NaCl at pH 3.0 (10 mM diglycine buffer). (B) Electron micrograph of the acid-induced denatured state of EqTxII at pH 1.2 and 25 °C.

Kinetics of Oligomer Formation. Figure 10 shows the time dependences of the molar ellipticity of EqTxII at 275 (panel A) and 220 nm (panel B) measured at 50 °C. In the absence of salt, the molar ellipticities of EqTxII at 275 and 220 nm are time-independent. By contrast, at 100 mM NaCl, $[\theta]_{275}$ increases, while $[\theta]_{220}$ decreases with time. Inspection of Figure 10C reveals that the observed decrease in $[\theta]_{220}$ reflects formation of a non-native secondary structure which shifts the far-UV CD spectrum of the protein to more negative values. It is difficult to resolve the contributions of inter- and intramolecular interactions to the association-induced formation of non-native secondary structure. To clarify this point, we have used native gel electrophoresis that can yield information about the size of the aggregates. Our native electrophoretograms obtained for EqTxII prein-

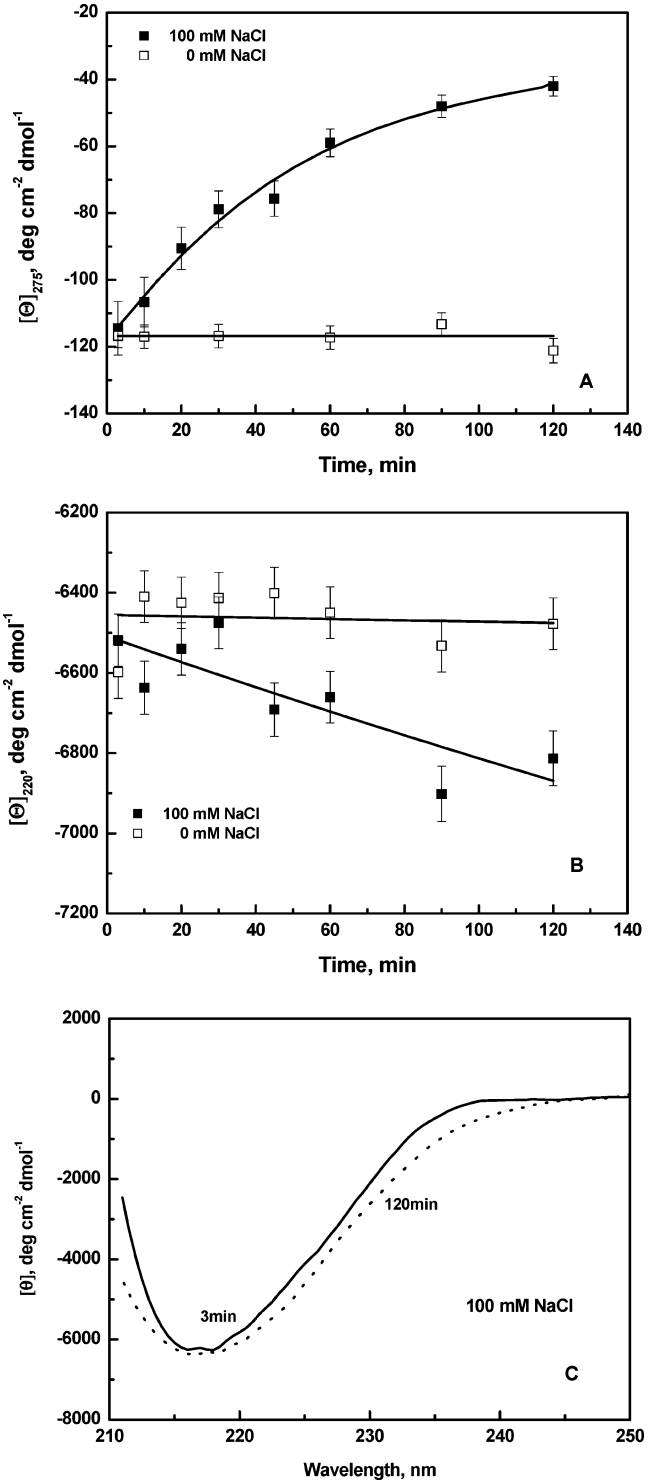

FIGURE 10: (A) Time dependence of the molar ellipticity of EqTxII at 275 nm preheated to 50 °C in the absence of salt (□) or with 100 mM NaCl (■). (B) Time dependence of the molar ellipticity of EqTxII at 220 nm preheated to 50 °C in the absence of salt (□) or with 100 mM NaCl (■). (C) Far-UV CD spectra of EqTxII at 100 mM NaCl. The toxin samples have been preincubated at 50 °C for 3 (—) and 120 min (···).

cubated at 50 °C suggest that, at 100 mM NaCl, the fraction of water-soluble oligomeric species of EqTxII depends on the time of incubation (see Figure 11). On the other hand, in the absence of salt, EqTxII remains monomeric at these temperatures. Our PAGE results further suggest that EqTxII oligomerization starts within 5−10 min of incubation at 50 °C, while in 2 h, oligomers begin to dominate the toxin

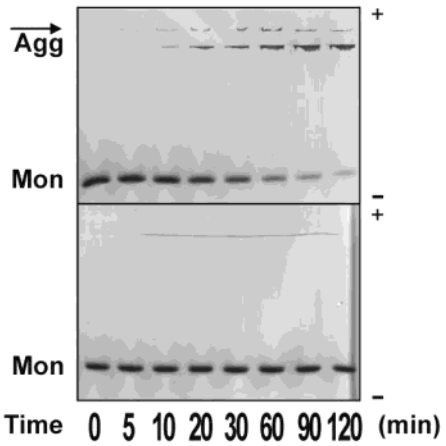

FIGURE 11: Native PAGE electrophoretogram of EqTxII preincubated for different periods of time at 50 °C in the presence of 100 mM NaCl (top half) and in the absence of salt (bottom half) at pH 3.0 (10 mM diglycine buffer).

population. This observation is supported by our CD spectroscopic results (Figure 10).

Results presented here in conjunction with our previously published data (*10*, *13*) indicate that EqTxII is prone to oligomerization under mild denaturing conditions. We do not yet know what components of the EqTxII structure participate in oligomer formation. EqTxII is a single-domain protein (*32*). Therefore, the mechanism of three-dimensional domain swapping observed for a number of multidomain proteins, including diphtheria toxin (*51*), can be safely ruled out. Instead, as a working hypothesis, we propose that, under denaturing conditions, the N-terminal segment, including an amphiphilic α-helix, dissociates from the *β*-sandwich core, thereby exposing its constituting nonpolar groups to the solvent. In fact, dissociation of the N-terminus has been shown to accompany interactions of the toxin with lipid membranes (*15*). It has been also reported that N-truncation of EqTx II greatly reduces the protein solubility (*56*). It is conceivable, therefore, that oligomerization proceeds with apolar "head-to-tail" association of partially unfolded EqTxII molecules and is accompanied by "hanging out" of the N-terminal α-helix. Alternatively, one may suggest that ordered oligomers are formed via continuous intermolecular *β*-sheet structures analogous to pneumolysin domain IV (*50*).

CONCLUDING REMARKS

Our current understanding of the mechanisms of toxin-induced pore formation in membranes has been primarily derived from structural studies on bacterial proteins. When binding to and inserting into the membrane, a pore-forming protein may undergo a series of structural changes that ultimately may bring about protein oligomerization. In this context, the pore-forming toxic action of EqTxII is believed to involve its trimerization or tetramerization. In this work, we have demonstrated that, in the presence of NaCl, EqTxII aggregates under mildly denaturing conditions. Significantly, our results suggest that these oligomeric structures consist of partially unfolded protein species. The partially unfolded conformational state of EqTxII is characterized by the lack of rigid tertiary structure, while exhibiting a well-defined secondary structure with enhanced α-helical content. Oligomerization of EqTx II is irreversible, while oligomerized, partially unfolded EqTxII molecules are hemolytically inac-

tive. On the basis of this observation, we suggest that, when performing its biological function, the toxin binds to the target membrane as a monomer and then oligomerizes at or within the membrane surface. Inspection of the recently determined crystal structure of EqTxII suggests that residues 1−17, 45−53, and 83−94 represent the largest segments that are potentially capable of adopting an alternative α-helical secondary structure (*32*). The observed enhancement of the α-helical content of the partially unfolded state EqTxII with its subsequent oligomerization suggests that the N-terminal domain containing residues 1−17 may be involved in these processes. It has been suggested that the N-terminal domain is directly involved in perforating a membrane, whereas the *β*-sandwich structure remains structurally unaltered during pore formation (*32*). Our results presented in this work support this mechanism.

ACKNOWLEDGMENT

We thank Mr. Luka Malenšek for his help with electron microscopy.

REFERENCES

1. Gouaux, E. (1997) Channel-forming toxins: tales of transformation, *Curr. Opin. Struct. Biol. 7*, 697−701.
2. Heuck, A. P., Tweten, R. K., and Johnson, A. E. (2001) *β*-Barrel pore-forming toxins: Intriguing dimorphic proteins, *Biochemistry 40*, 9065−9073.
3. Anderluh, G., and Maček, P. (2002) Cytolytic peptide and protein toxins from sea anemones (Anthozoa: Actinaria), *Toxicon 40*, 111−124.
4. Zorec, R., Tester, M., Maček, P., and Mason, W. T. (1990) Cytotoxicity of equinatoxin II from the sea anemone *Actinia equina* involves ion channel formation and an increase in intercellular calcium activity, *J. Membr. Biol. 118*, 243−249.
5. Belmonte, G., Pederzolli, C., Maček, P., and Menestrina, G. (1993) Pore formation by the sea-anemone cytolysin equinatoxin-II in red-blood-cells and model lipid-membranes, *J. Membr. Biol. 131*, 11−22.
6. Malavašič, M., Poklar, N., Maček, P., and Vesnaver, G. (1996) Fluorescence studies of the effect of pH, guanidine hydrochloride and urea on equinatoxin II conformation, *Biochim. Biophys. Acta 1280*, 65−72.
7. Poklar, N., Lah, J., Salobir, M., Maček, P., and Vesnaver, G. (1997) pH and temperature-induced molten-globule like denatured states of equinatoxin II: A study by UV-melting, DSC, far- and near-UV CD spectroscopy, and ANS fluorescence, *Biochemistry 36*, 14345−14352.
8. Alvarez, C., Pazos, I. F., Lanio, M. E., Martinez, D., Schrier, S., Casallanovo, F., Campos, A. M., and Lissi, E. (2001) Effect of pH on the conformation, interaction with membranes and hemolytic activity of sticholysin II, a pore forming cytolysin from the sea anemone *Stichodactyla helianthus*, *Toxicon 39*, 539−553.
9. Mancheno, J. M., De Los Rios, V., Martinez Del Pozo, A., Lanio, M. E., Onadera, M., and Gavilanes, J. G. (2001) Partially folded states of the cytolytic protein sticholysin II, *Biochim. Biophys. Acta 1545*, 122−131.
10. Poklar, N., Völker, J., Anderluh, G., Maček, P., and Chalikian, T. V. (2001) Acid- and base-induced conformational transitions of equinatoxin II, *Biophys. Chem. 90*, 103−121.
11. Martinez, D., Campos, A. M., Pazos, F., Alvarez, C., Lanio, M. E., Casallanovo, F., Schreier, S., Salinas, R. K., Vergara, C., and Lissi, E. (2001) Properties of St I and St II, two isotoxins isolated from *Stichodactyla heliantus*: a comparison, *Toxicon 39*, 1547−1560.
12. Hinds, M. G., Zhang, W., Anderluh, G., Hansen, P. E., and Norton, R. S. (2002) Solution structure of the eukaryotic pore-forming cytolysin equinatoxin II: implications for pore formation, *J. Mol. Biol. 5*, 1219−1229.
13. Poklar, N., Fritz, J., Maček, P., Vesnaver, G., and Chalikian, T. V. (1999) Equinatoxin interactions with model lipid membranes: A calorimetric and spectroscopic study, *Biochemistry 38*, 14999−15008.
14. Caaveiro, J. M. M., Echabe, I., Gutierrez-Aguirre, I., Nieva, J. L., Arrondo, J. L. R., and Gonzales-Manas, J. M. (2001) Differential interaction of equinatoxin II with model membranes in response to lipid composition, *Biophys. J. 80*, 1343−1353.
15. Hong, Q., Gutierrez-Aguirres, I., Barlič, A., Malovrh, P., Kristan, K., Podlesek, Z., Maček, P., Turk, D., Gonzales-Manas, J., Lakey, J. H., and Anderluh, G. (2002) Two-step membrane binding by equinatoxin II, a pore-forming toxin from the sea anemone, involves an exposed aromatic cluster and a flexible helix, *J. Biol. Chem. 277*, 41916−41924.
16. Anderluh, G., Barlič, A., Podlesek, Z., Maček, P., Pungerčar, J., Gubenšek, F., Zecchini, M. L., Della Serra, M., and Manesstrina, G. (1999) Cysteine-scanning mutagenesis of an eukaryotic pore-forming toxin from sea anemone. Topology in lipid membrane, *Eur. J. Biochem. 263*, 128−136.
17. Eilers, M., Hwang, S., and Schatz, G. (1988) Unfolding and refolding of a purified precursor protein during import into isolated mitochondria, *EMBO J. 7*, 1139−1145.
18. Endo, T., and Shatz, G. (1988) Latent membrane perturbation activity of a mitochondrial precursor protein is exposed by unfolding, *EMBO J. 7*, 1153−1158.
19. van der Goot, F. G., Gonzales-Manas, J. M., Lakey, J. H., and Pattus, F. (1991) A "molten-globule" membrane insertion intermediate of the pore-forming domain of colicin A, *Nature 354*, 408−410.
20. de Young, L. R., Fink, A. L., and Dill, K. A. (1993) Aggregation and denaturation of apomyoglobin in aqueous urea solutions, *Biochemistry 32*, 3877−3886.
21. Bychkova, V. E., Dujsekina, A. E., Klemin, S. I., Tiktopulo, E. I., Uversky, V. N., and Ptitsyn, O. B. (1996) Molten globule-like state of cytochrome *c* under conditions simulating those near the membrane surface, *Biochemistry 35*, 6058−6063.
22. Maček, P., and Lebez, D. (1988) Kinetic of hemolysis induced by equinatoxin, a cytolitic toxin from sea anemone *Actinia equina*. Effect of some ions and pH, *Toxicon 26*, 441−445.
23. Provencher, S. W., and Glöckner, J. (1981) Estimation of globular protein secondary structure from circular dichroism, *Biochemistry 20*, 33−37.
24. Marky, L. A., and Breslauer, K. J. (1987) Calculating thermodynamic data for transitions of any molecularity from equilibrium melting curves, *Biopolymers 26*, 1601−1620.
25. Eggers, F., and Funck, T. (1973) Ultrasonic measurements with millilitre liquid samples in the 0.5−100 MHz range, *Rev. Sci. Instrum. 44*, 969−978.
26. Sarvazyan, A. P. (1982) Development of methods of precise ultrasonic measurements in small volumes of liquids, *Ultrasonics 20*, 151−154.
27. Eggers, F. (1992) Ultrasonic velocity and attenuation measurements in liquids with resonator, extending the MHz frequency range, *Acustica 76*, 231−240.
28. Sarvazyan, A. P., Selkov, E. E., and Chalikian, T. V. (1988) Constant-path acoustic interferometer with transition layers for precision measurements in small liquid volumes, *Sov. Phys. Acoust. 34*, 631−634.
29. Sarvazyan, A. P., and Chalikian, T. V. (1991) Theoretical analysis of an ultrasonic interferometer for precise measurements at high pressures, *Ultrasonics 29*, 119−124.
30. Geourjon, C., and Deléage, G. (1995) SOPMA: Significant improvement in protein secondary structure prediction by consensus prediction from multiple alignments, *Cabios 11*, 681−684.
31. Jones, D. T. (1999) Protein secondary structure prediction based on position-specific scoring matrices, *J. Mol. Biol. 292*, 195−202.
32. Athanasiadis, A., Anderluh, G., Maček, P., and Turk, D. (2001) Crystal structure of the soluble form of equinatoxin II from the sea anemone *Actinia equina*, *Structure 9*, 341−346.
33. Semisotnov, G. V., Rodionova, N. A., Razgulyaev, O. I., Uversky, V. N., Gripas, A. F., and Gilmanshin, R. I. (1991) Study of the molten globule intermediate state in protein folding by a hydrophobic fluorescent-probe, *Biopolymers 31*, 119−129.
34. Ali, V., Prakash, K., Kulkarni, S., Ahmad, A., Mathusudan, K. P., and Bhakuni, V. (1999) 8-Anilino-1-naphthalene sulfonic acid (ANS) induces folding of acid unfolded cytochrome *c* to molten globule state as a result of electrostatic interactions, *Biochemistry 38*, 13635−13642.

35. Matulis, D., Baumann, C. G., Bloomfield, V. A., and Lovrien, R. E. (1999) 1-Anilino-8-naphthalene sulfonate as a protein conformational tightening agent, *Bioploymers 49*, 451−458.
36. Khoo, H. E., Fong, C. L., Yuen, R., and Chen, D. (1997) Stimulation of haemolytic activity of sea anemone cytolysins by 8-anilino-1-naphthalene sulphonate, *Biochem. Biophys. Res. Commun. 232*, 422−426.
37. Belmonte, G., Menestrina, G., Pederzolli, C., Križaj, I., Gubensek, F., Turk, T., and Maček, P. (1994) Primary and secondary structure of a pore-forming toxin from the sea anemone, *Actinia equina L.*, and its association with lipid vesicles, *Biochim. Biophys. Acta 1192*, 197−204.
38. Ramalingam, K., Aimoto, S., and Bello, J. (1992) Conformational studies of anionic melittin analogues: Effect of peptide conformation, pH, ionic strength, and temperature: models for protein folding and halophillic proteins, *Biopolymers 32*, 981−992.
39. Uversky, V. N., Segel, D. J., Doniach, S., and Fink, A. L. (1998) Association-induced folding of globular proteins, *Proc. Natl. Acad. Sci. U.S.A. 95*, 5480−5483.
40. Uversky, V. N., Karnoup, A. S., Khurana, R., Segel, D. J., Doniach, S., and Fink, A. L. (1999) Association of partially-folded intermediates of staphylococcal nuclease induces structure and stability, *Protein Sci. 8*, 161−173.
41. Chalikian, T. V. (2003) Volumetric properties of proteins, *Annu. Rev. Biophys. Biomol. Struct. 32*, 207−235.
42. Tanford, C. (1968) Protein denaturation, *Adv. Protein Chem. 23*, 121−282.
43. London, J., Skrzynia, C., and Goldberg, M. E. (1974) Renaturation of *Escherichia coli* tryptophanase after exposure to 8 M urea. Evidence for existence of nucleation centers, *Eur. J. Biochem. 47*, 409−415.
44. Mitraki, A., and King, J. (1989) Protein folding intermediates and inclusion body formation, *Bio/Technology 7*, 690−697.
45. Elizer, D., Chiba, K., Tsuruta, H., Doniach, S., Hodgson, K. O., and Kihara, H. (1993) Evidence of an associative intermediate on the myglobin refolding pathway, *Biophys. J. 65*, 912−917.
46. Oberg, K., Chreenyk, B. A., Wetsel, R., and Fink, A. L. (1994) Native secondary structure in interleukin-1β inclusion bodies by attenuated total reflectance FTIR, *Biochemistry 33*, 2628−2634.
47. Fink, A. L. (1995) Compact intermediate states in protein folding, *Annu. Rev. Biophys. Biomol. Struct. 24*, 495−522.
48. Fink, A. L. (1998) Protein aggregation: folding aggregates, inclusion bodies and amyloid, *Folding Des. 3*, R9−R15.
49. Ptitsyn, O. B. (1995) Molten globule and protein folding, *Adv. Protein Chem. 47*, 83−229.
50. Gilbert, J. C. R., Rossjohn, J., Parker, M. W., Tweten, R. K., Morgan, P. J., Mitchell, T. J., Errington, N., Rowe, A. J., Andrew, P. W., and Byron, O. (1998) Self-interaction of pneumolysin, the pore-forming protein toxin of *Streptococcus pneumonia*, *J. Mol. Biol. 284*, 1223−1237.
51. Steere, B., and Eisenberg, D. (2000) Characterization of High-Order Diphteria Toxin Oligomers, *Biochemistry 39*, 15901−15909.
52. Kelly, J. W. (1998) The alternative conformations of amyloidogenic proteins and their multi-step assembly pathways, *Curr. Opin. Struct. Biol. 8*, 101−106.
53. Rossjohn, J., Gilbert, R. J. C., Craane, D., Morgan, P. J., Mitchell, T. J., Rowe, A. J., Andrew, P. W., Tweten, R. K., and Parker, M. W. (1998) The molecular mechanism of pneumolysin, a virulence factor from *Streptococcus pneumonniae*, *J. Mol. Biol. 284*, 449−461.
54. Petosa, C., Collier, R. J., Klimpel, K. R., Leppla, S. H., and Liddington, R. C. (1997) Crystal structure of the antrax toxin protective antigen, *Nature 385*, 833−838.
55. Song, L., Hobaugh, M. R., Shustak, C., Cheley, S., Bayley, H., and Gouaux, J. E. (1996) Structure of staphylococcal α-hemolysin, a heptameric transmembrane pore, *Science 274*, 1859−1866.
56. Anderluh, G., Pungerčar, J., Križaj, I., Štrukelj, B., Gubenšek, F., and Maček, P. (1997) N-Terminal truncation mutagenesis of equinatoxin II, a pore-forming protein from the sea anemone *Actinia equina*, *Protein Eng. 10*, 751−755.

BI049616H